

## Electron radiation-induced degradation of silicon solar cells



Guo Li <sup>a</sup>, Chukwuka Madumelu <sup>a</sup>, Michael Kelzenberg <sup>c</sup>, Peter Toth <sup>b</sup>, Gavin Conibeer <sup>a,b</sup>, Bram Hoex <sup>a,\*</sup>

<sup>a</sup> School of Photovoltaic and Renewable Energy Engineering, University of New South Wales, Sydney, NSW, 2052, Australia

<sup>b</sup> Extraterrestrial Power Pty Ltd, Cronulla, 2230, New South Wales, Australia

<sup>c</sup> Applied Physics & Materials Science, California Institute of Technology, Pasadena, CA, 91125, United States

### ABSTRACT

Silicon solar cells have attracted increasing interest for space exploration due to their significant cost-effectiveness compared to other photovoltaic technologies. However, performance of current commercial silicon solar cell architectures under space conditions, such as electron irradiation, has not been investigated. This work evaluates the electrical performance of n-type lifetime wafers and state-of-the-art silicon solar cells, including p-type passivated emitter and rear contact (PERC) and n-/p-type tunnel oxide passivated contact (TOPCon) silicon solar cells, after electron irradiation. These samples were irradiated under varying doses of 1-MeV electrons and  $2.16 \times 10^{14}$  e/cm<sup>2</sup> of 5-MeV electrons. Post-radiation characterisation reveals a significant reduction in minority carrier lifetime, which was predominantly attributed to the bulk lifetime degradation from  $\sim 75,000$   $\mu$ s to  $\sim 240$   $\mu$ s after  $10^{12}$  e/cm<sup>2</sup> and further to  $\sim 0.2$   $\mu$ s after  $10^{15}$  e/cm<sup>2</sup> of 1-MeV electron irradiation. Corresponding to the reduction in bulk lifetime, the integrated external quantum efficiency (EQE) decreased by 27.5 % for p-PERC and 33.3 % for n-TOPCon solar cells relative to their initial value. Furthermore, defect characterisation using the defect parameterisation solution space (DPSS) method identifies the vacancy-vacancy as the dominant radiation-induced defect. Ultimately, comparative analysis with actual space mission data suggests that the observed degradation under  $5 \times 10^{14}$  e/cm<sup>2</sup>, 1-MeV electron irradiation is comparable to 3–5 years of low Earth orbit (LEO) space conditions. These findings underscore the critical role of minority bulk carrier lifetime degradation in limiting the performance of silicon solar cells under a space radiation environment, and highlight the need for enhanced radiation tolerance in commercial space silicon solar cells.

### 1. Introduction

In recent years, silicon solar cells have attracted increasing attention for low Earth orbit (LEO) space applications, such as Starlink satellites, thanks to their significant cost-effectiveness. Current state-of-the-art commercial photovoltaic products with heterojunction (HJT) and tunnel oxides and passivated contact (TOPCon) structures have demonstrated power conversion exceeding 25 % under the AM1.5G spectrum [1–3], which is equivalent to  $\sim 23$  % under the AM0 spectrum [4]. As the module cost has dropped down to 0.1 USD/W [5], silicon technology has now again become an appealing solution for cost-sensitive, short-duration missions, such as on constellation satellites in LEO.

Research on space silicon solar cells up to the 2000s primarily concentrated on thin, high-efficiency designs, driven by silicon's inherently limited tolerance to radiation [6–9]. After this period, the focus was predominantly on III-V solar cells, which had a significantly higher defect tolerance [8]. As of 1998, the champion space-specialised silicon solar cells were reported by SHARP Corporation and the National Space Development Agency of Japan (NASDA), which incorporated a 100  $\mu$ m cell thickness with a non-reflective surface/localised back

surface field (NRS/LBSF) design [10,11]. This space solar cell achieved an AM0 efficiency of  $\sim 17$  % and retained  $\sim 70$  % of its beginning-of-life (BoL) performance after being exposed to a dose of  $10^{15}$  e/cm<sup>2</sup> 1 MeV electrons. In recent years, silicon solar cells have regained considerable interest due to their continuous improvements in cell efficiency and significant cost reduction. Simulation studies by Ma et al. [12] have demonstrated that the modern TOPCon silicon solar cells offer advantages over conventional cell structures after electron radiation, owing to the full area contact design. Moreover, experimental work by Khan et al. [13] suggests that hydrogen atoms, commonly introduced during passivation, can effectively mitigate radiation-induced defects in silicon. These studies suggest pathways to enhance radiation tolerance of future silicon solar cells. In industry, the ultrathin HJT silicon solar cell produced by Solestial Inc [14,15] exhibited superior recovery capabilities, effectively healing electron radiation damage at temperature above 65 °C. These studies suggest pathways to enhance radiation tolerance of future silicon solar cells. However, the radiation tolerance of modern silicon solar cell architectures has not been comprehensively studied, compared and reported, which is critical to further optimising these cells for space applications.

\* Corresponding author.

E-mail address: [b.hoex@unsw.edu.au](mailto:b.hoex@unsw.edu.au) (B. Hoex).

This study characterises the performance of state-of-the-art silicon wafers and cells before and after exposure to electron irradiation at different fluences and energy settings. The radiation-induced defects were then characterised via the DPSS and temperature and injection-dependent lifetime spectroscopy (TIDLS) [16] for n-TOPCon lifetime wafers. Furthermore, a detailed analysis was conducted on short-circuit current density ( $J_{sc}$ ), open-circuit voltage ( $V_{oc}$ ), cell efficiency, EQE, and effective minority carrier lifetime ( $\tau$ ) of silicon solar cells after exposure to various electron irradiation doses and energies. Finally, by comparing simulated radiation results with actual flight data of the same p-PERC silicon solar cell, this study confirmed that an electron irradiation dose of  $5 \times 10^{14} \text{ e/cm}^2$  corresponds to approximately 3–5 years in a LEO space environment.

## 2. Experimental Configuration

Figs. 1 and 3 show the experimental workflow of the 1 MeV and 5 MeV batches. In the 1 MeV batch experiment, n-type silicon lifetime wafers ( $1 \Omega \text{ cm}$ ,  $158 \times 158 \text{ mm}^2$ ) with a symmetrical TOPCon structure design (see Fig. 2) and  $158 \times 158 \text{ mm}^2$  n-TOPCon-1 silicon solar cell were used. They were exposed to 1 MeV electron irradiation at doses ranging from  $10^{12}$  to  $10^{15} \text{ e/cm}^2$ . Simultaneously, commercial n-TOPCon and p-PERC silicon solar cells were irradiated with 1 MeV electrons at doses ranging from  $10^{14} \text{ e/cm}^2$  and  $5 \times 10^{14} \text{ e/cm}^2$ .

The minority carrier lifetime measurements were carried out before and after the irradiation process using a Sinton WCT-120 lifetime tester, and photoluminescence (PL) images were obtained with a LIS-R3 PL Imager to evaluate the uniformity and severity of radiation damage to lifetime wafers. The surface recombination current  $J_0$  was extracted at high minority carrier injection levels using [17]:

$$\tau_{s,J_0}^{-1} = 2J_0 \times \frac{N_{doping} + \Delta n}{qWn_i^2} \quad \text{Eq. 2.1}$$

where the  $\tau_{s,J_0}$  is the effective carrier lifetime due to surface recombination,  $N_{doping}$  is the net dopant density,  $\Delta n$  is the excess carrier density,  $q$  is the elementary charge,  $W$  is the wafer thickness of the sample and  $n_i$  is the intrinsic carrier concentration of silicon. Furthermore, the measured injection-dependent lifetime spectroscopy (IDLS) curves were later fitted to extract corresponding  $J_0$ , and bulk SRH lifetime ( $\tau_{SRH,bulk}$ ) based on the following equations [18–20],

$$\tau_{eff}^{-1} = \tau_{rad}^{-1} + \tau_{Auger}^{-1} + \tau_{s,J_0}^{-1} + \tau_{SRH,bulk}^{-1} \quad \text{Eq. 2.2}$$

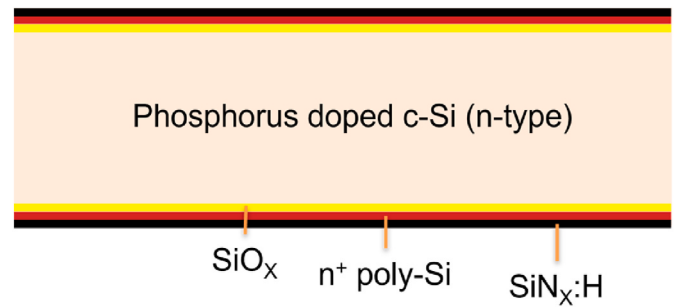


Fig. 2. Silicon wafer with symmetric TOPCon structure used in this work.

$$\tau_{Auger}^{-1} = C_{n,eff} n_0 \left( \frac{np - n_{i,eff}}{\Delta n} \right) + C_{p,eff} n_0 \left( \frac{np - n_{i,eff}}{\Delta n} \right) + C_a \Delta n^{0.92} \left( \frac{np - n_{i,eff}}{\Delta n} \right) \quad \text{Eq. 2.3}$$

$$\tau_{rad}^{-1} = \frac{\Delta n}{B(np - n_{i,eff}^2)} \quad \text{Eq. 2.4}$$

$$\tau_{SRH,bulk}^{-1} = \tau_m + \tau_M \frac{\Delta n}{\Delta n + N_M} \quad \text{Eq. 2.5}$$

here, the  $C_{n,eff}$  and  $C_{p,eff}$  are the effective Auger recombination coefficients for electrons and holes, respectively,  $C_a$  is an empirical Auger coefficient accounting for high-injection effects,  $n_0$  is the equilibrium majority carrier concentration,  $n$  and  $p$  are the total electron and hole concentrations and  $n_{i,eff}$  is the effective intrinsic carrier concentration. For radiative recombination,  $B$  is the radiative recombination coefficient. For SRH recombination,  $\tau_m$  and  $\tau_M$  are the minority and majority carrier lifetime and  $N_M$  is the majority carrier concentration (dopant density).

The lifetime of irradiated wafers was also measured at temperatures of  $30^\circ \text{C}$ ,  $65^\circ \text{C}$  and  $100^\circ \text{C}$  to characterise the radiation-induced defects by using TIDLS/DPSS method. In addition to the lifetime test samples, two types of commercial silicon solar cells ( $158 \times 158 \text{ mm}^2$  p-PERC and n-TOPCon) were characterised for their electrical performance after exposure to electron irradiation doses of  $10^{14}$  and  $10^{15} \text{ e/cm}^2$  1 MeV electrons.

In addition to the 1 MeV irradiation, three types of commercial silicon solar cells, including  $158 \times 158 \text{ mm}^2$  p-PERC,  $166 \times 166 \text{ mm}^2$  p-TOPCon and six different n-TOPCon solar cells, were exposed to  $2.16 \times 10^{14} \text{ e/cm}^2$  of 5 MeV electron irradiation as shown in Fig. 3. Although

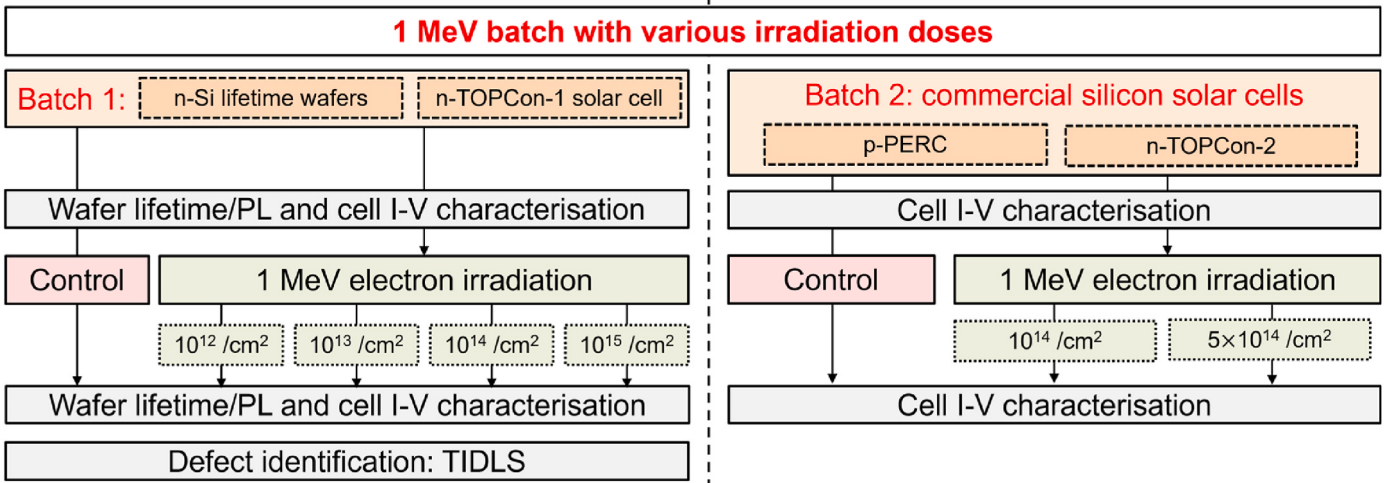


Fig. 1. Experimental workflow for the 1 MeV irradiation batch.

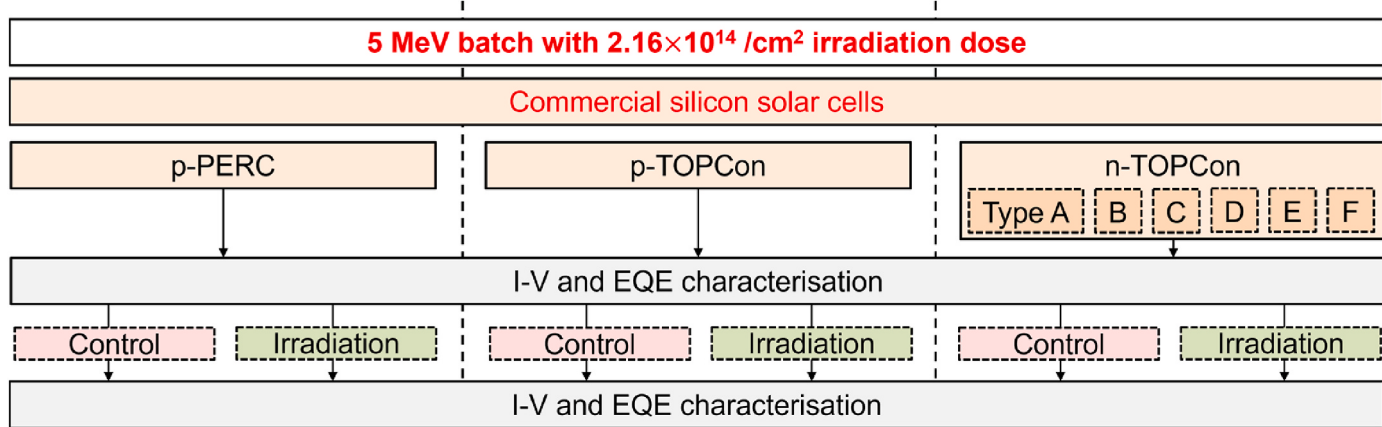


Fig. 3. Experimental workflow for 5 MeV irradiation batch.

the electron energy differs, the degradation of p-PERC silicon solar cell by 5 MeV irradiation was found to be comparable to that observed under 1 MeV conditions at a  $5 \times 10^{14} e/cm^2$ , due to similar non-ionising energy loss (NIEL) such as atomic displacements [21–23]. According to previous findings [6], the radiation damage caused by  $\sim 10^{14} e/cm^2$  5 MeV electrons is likely the same as the  $5 \times 10^{14} e/cm^2$  1 MeV irradiation for a p-type silicon solar cell.

Six n-TOPCon solar cells fabricated by different manufacturers in 2021–2024 were tested to provide a more comprehensive analysis of the radiation-induced degradation of n-TOPCon performance. The rear junction p-TOPCon solar cell had the same cell structure as the n-TOPCon, with gallium replacing phosphorus as the bulk dopant. The 5 MeV-electron-irradiated cells were measured using similar techniques to those employed in the 1 MeV batch to evaluate performance degradation caused by different electron irradiation.

The remaining performance (or remaining factor, RF) was used to quantitatively compare the performance degradation after irradiation, and the trend of RF after different irradiation doses can be estimated with an empirical equation [24,25]:

$$RF = 1 - C \log\left(1 + \frac{\phi}{\phi_0}\right) \quad \text{Eq. 2.6}$$

where  $\phi$  is the accumulated irradiation dose that was applied to silicon solar cells, and  $C$  and  $\phi_0$  are the fitting parameters. The fitting parameter  $C$  reflects the intrinsic radiation sensitivity of the solar cells and should remain constant among tested samples, as they are from the same batch of p-PERC silicon solar cells. In contrast, the  $\phi_0$  was expected to vary between different samples due to the effectiveness of different shielding method, which varies the actual electron fluences reaching the p-PERC silicon solar cell.

The I-V characterisation was conducted using PVTools LOANA cell tester for AM1.5G spectrum and using a Wavelabs SINUS-220 I-V tester for AM0 spectrum. The AM0 I-V results were compared with data obtained during the actual space mission. In addition, the EQE was measured using a PV Measurements QEX7 Spectral Response tool. Quokka 3 was employed to simulate optical response, carrier transport and recombination in the silicon solar cells with the drift-diffusion model [26]. The software uses conductive boundary conditions to represent doped surfaces and contact layers, enabling accurate electrical modelling of the complete solar cell structure without detailed meshing each layer. The simulations were calibrated using measured cell parameters to ensure consistency with experimental conditions. Accordingly, the experimental EQE curves were fitted using Quokka 3 to extract the optical parameters of the tested samples [27–30]. The efficiency of these silicon solar cells was then simulated as a function of bulk lifetime based on experimental results and fitted optical parameters to evaluate

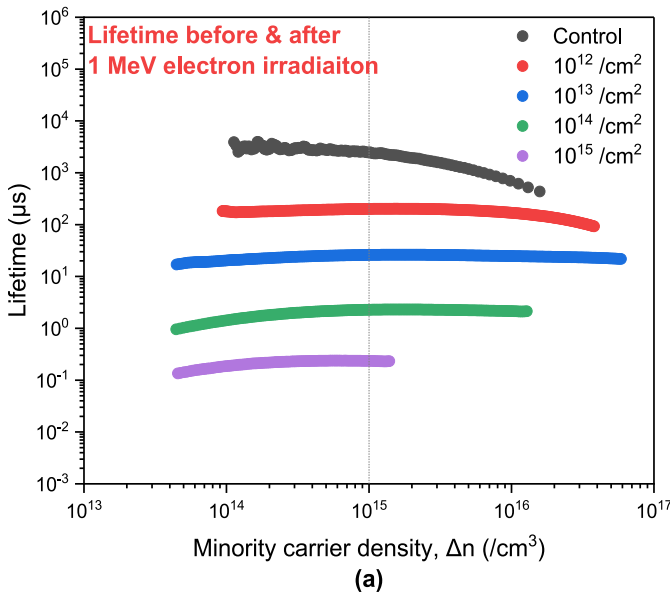
their performance potential.

A calibration experiment was performed that involved similar laser-cut p-PERC solar cells that were deployed as part of Caltech's SPACE Solar Power Demonstrator (SSPD-1) mission at  $\sim 500$  km altitude for  $\sim 7$  months [31], which allowed us to access the real-time cell performance during a LEO space operation and compare it with the degradation observed in the lab. In this mission, three similar p-PERC silicon solar cells were encapsulated differently, including one bare cell, one with four  $\mu m$  of polyimide and one with a traditional ceria-doped cover glass structure ( $70-\mu m$  CMG/ $75-\mu m$  DC 93–500). The temperature of these cells during the mission was monitored to be between  $-20^\circ C$  to  $40^\circ C$ . Thus, it is assumed that these solar cells did not undergo any recovery under such low-temperature conditions during the short duration of the mission (7 months).

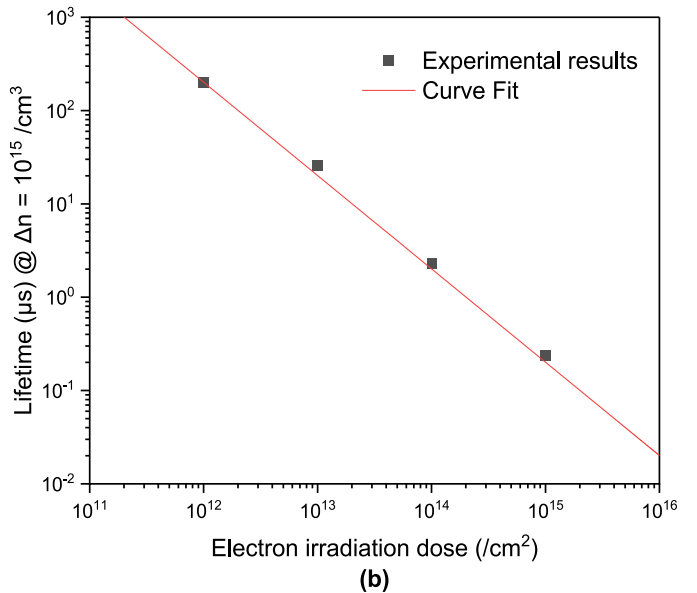
### 3. Results and discussion

#### 3.1. Silicon solar wafers after 1 MeV electron irradiation

The lifetime curves of n-TOPCon wafers are shown in Fig. 4 (a), including non-irradiated (control) and irradiated samples with a total electron dose ranging from  $10^{12}$  to  $10^{15} e/cm^2$ . In the control samples, the effective lifetime showed a decreasing trend with increasing minority carrier injection density and was found to be  $\sim 3300 \mu s$  and  $\sim 430 \mu s$  at  $1.13 \times 10^{14}/cm^3$  and  $1.58 \times 10^{16}/cm^3$ , respectively. This injection dependence was attributed to the high Auger recombination loss at high injection levels. Following a  $10^{12}$  and  $10^{13} e/cm^2$  1 MeV electron irradiation dose, the Auger recombination became less significant, where the minority carrier lifetime degraded to an average value of  $\sim 174 \mu s$  and  $\sim 23.9 \mu s$ , respectively. With higher irradiation doses up to a  $10^{15} e/cm^2$ , the lifetimes were further reduced to  $\sim 2.04 \mu s$  in the  $10^{14} e/cm^2$  samples and  $\sim 0.21 \mu s$  in the  $10^{15} e/cm^2$  samples. However, it should be noted that the highest injection density was only around  $10^{15}/cm^3$  in the samples with  $10^{15} e/cm^2$  electron irradiation due to the low bulk lifetime and limits in the generation rate of the photoconductance tool used. To present a clearer trend of lifetime degradation with higher doses of irradiation damage, their effective lifetimes at  $\Delta n = 10^{15}/cm^3$  are presented in Fig. 4 (b). It is clear that a higher irradiation dose of electron flux can result in a significantly lower effective lifetime down to  $\sim 0.2 \mu s$  in the irradiated n-type silicon wafers. The lifetime degradation trend follows an inverse power-law relationship ( $Y = a X^{-b}$ ), where every order of magnitude increase in irradiation dose leads to an approximately one-order-of-magnitude decrease in the effective lifetime ( $\Delta n = 10^{15}/cm^3$ ). Meanwhile, samples exposed to high-dose irradiation (e.g.  $10^{15} e/cm^2$ ) exhibited an extremely low lifetime ( $\sim 0.2 \mu s$ ), likely due to the overwhelming bulk recombination losses. As a result, this made it difficult to obtain reliable high-injection lifetime data for surface



(a)



(b)

**Fig. 4.** (a) Effective minority carrier lifetime of the TOPCon silicon wafers after exposure to different doses of 1 MeV electron irradiation, (b) experimental and fitted lifetime at  $\Delta n = 10^{15}/\text{cm}^3$ .

recombination analysis.

To further evaluate the potential changes in surface recombination from the irradiation damage, Fig. 5 shows the surface  $J_0$  analysis for both control and irradiated wafers based on Eq. (2.1). Only  $10^{12} \text{ e/cm}^2$  and  $10^{13} \text{ e/cm}^2$  results are presented in the irradiated batch since the lifetime at a high injection level cannot be obtained for the heavily irradiated wafers, as presented in Fig. 4. Based on the fitted results at a high injection level, the surface recombination current,  $J_0$ , of the control sample was around  $61 \text{ fA/cm}^2$ , whereas in the irradiated samples, the  $J_0$  values were  $88 \text{ fA/cm}^2$  and  $49 \text{ fA/cm}^2$  after  $10^{12} \text{ e/cm}^2$  and  $10^{13} \text{ e/cm}^2$  doses of 1 MeV electron irradiation, respectively. Consequently,  $J_0$  was found to be relatively constant, indicating that most radiation-induced lifetime degradation was likely associated with bulk lifetime degradation rather than the surface. The performance losses will be further assessed in the subsequent sections.

In addition, the PL images are presented in Fig. 6 to evaluate the uniformity of the radiation damage. The PL intensity scales were set from 0 to 150,000 counts/s for non-irradiated wafers and 0 to 6000 counts/s for irradiated wafers due to the significantly low PL intensity observed after radiation. The average normalised PL intensity was approximately  $\sim 20,000$  counts/sec before the irradiation process. Following the 1 MeV and  $10^{12} \text{ e/cm}^2$  electron irradiation, it degraded to  $\sim 1000$  counts/sec and became lower than 120 counts/sec for the heavily irradiated wafers. Although the PL intensity of heavily irradiated samples could not be reliably measured due to the limited sensitivity of the PL instrument, the results from  $10^{12} \text{ e/cm}^2$  irradiated wafers demonstrate the uniformity of the irradiation damage. The observed scratches and laser engraving before irradiation are consistent with the patterns in the irradiated samples, indicating a uniform distribution of radiation damage across the solar wafers.

According to Eq. (2.2) – Eq. (2.5), the effective minority carrier lifetime was fitted for a non-irradiated control and an irradiated wafer exposed to  $10^{12} \text{ e/cm}^2$  of 1 MeV electrons using three fitting parameters, including  $J_0$ ,  $\tau_m$  and  $\tau_M$ . The  $\tau_{Aug}$  and  $\tau_{rad}$  were considered to be identical for both irradiated and non-irradiated samples, as they originated from the same silicon wafer. Accordingly, the fitted lifetime results are presented in Fig. 7 with  $R^2$  values of 0.997 for non-irradiated and 0.970 for irradiated samples.

As shown in Fig. 7(a), the fitted effective lifetime curve aligned well with the experimental results. The  $\tau_{eff}$  of the non-irradiated sample was dominated by  $\tau_{Aug}$  at high carrier injection level ( $\Delta n > 10^{15}/\text{cm}^3$ ), and

by both  $\tau_{Aug}$  and  $\tau_{J_0}$  at lower injection levels. In particular, at a  $10^{15}/\text{cm}^3$  minority carrier density ( $\Delta n$ ), the recombination lifetime components of the non-irradiated wafer were  $\sim 4.0 \text{ fA/cm}^2$  for  $J_{0,\text{fit}}$  and  $\sim 75,000 \mu\text{s}$  for  $\tau_{SRH,bulk}$ . The low fitted  $J_0$  is a result of the superior surface passivation quality of these lifetime samples, enabling the effective lifetime approaching the Auger limits at  $\Delta n > 10^{15}/\text{cm}^3$ , and the  $\tau_{eff}$  is  $\sim 3600 \mu\text{s}$  at  $10^{15}/\text{cm}^3$  injection level.

After the  $10^{12} \text{ e/cm}^2$  of 1 MeV electron irradiation, the  $\tau_{SRH,bulk}$  value became one magnitude lower compared to the non-irradiated sample, making it dominant at a carrier injection density at  $\Delta n$  up to  $\sim 10^{16}/\text{cm}^3$ . In particular, the  $\tau_{SRH,bulk}$  decreased to  $240 \mu\text{s}$  at  $\Delta n = 10^{15}/\text{cm}^3$ , which is over 300 times lower compared to the non-irradiated sample. In the meantime, the fitted  $J_0$  was  $30 \text{ fA/cm}^2$ . Although the fitted  $J_0$  results differed slightly between the two methods shown in Figs. 5 and 7, both showed minimal changes between before and after irradiation, suggesting the surface recombination was unaffected by the irradiation process. In contrast, the significant degradation in  $\tau_{SRH,bulk}$  indicates that the radiation damage in the silicon wafer is primarily attributed to losses within the substrate, which were caused by the radiation-induced bulk defects.

Subsequently, the defect parameters of the n-TOPCon lifetime wafer with  $10^{12} \text{ e/cm}^2$  of 1 MeV electron irradiation were characterised by using the TIDLS/DPSS method [16]. Fig. 8 (a) shows the linearised injection-dependent defect lifetime curve as a function of  $X = p/n$  at three different temperatures, along with linear curve fitting. These SRH lifetime curves are transformed into a linear form [18],  $\tau(X) = \left( 1 + \frac{k p_1 v_h}{n_0 v_e} \frac{n_1}{n_0} \right) + \left( \frac{k v_h}{v_e} \frac{k p_1 v_h}{n_0 v_e} \frac{n_1}{n_0} \right) X$ , where the slope and intercept related to the key defect parameters, including trap energy  $E_t$ , defect density  $N_t$ , hole capture cross section  $\sigma_h$ , and capture cross-section ratio  $k$ . The high linearisation observed in these curves suggests that the irradiated samples were predominantly affected by one single-level defect property ( $E_t$ ,  $N_t \sigma_h$  and  $k$ ).

Moreover, the DPSS results for  $E_t$ - $k$  curve are presented in Fig. 8 (b), which were used to extract the capture cross-section ratio and corresponding trap energy within the bandgap. Three possible defect parameters were identified based on the crossover points and are summarised in Table 1. Two possible candidates were observed on the upper half of the bandgap, with energy levels located at  $E_t - E_i = 0.55 \text{ eV}$  and  $k = 7 \times 10^{-5}$  for Option 1 and  $0.26 \text{ eV}$  and  $k = 2.63$  for Option 2. In

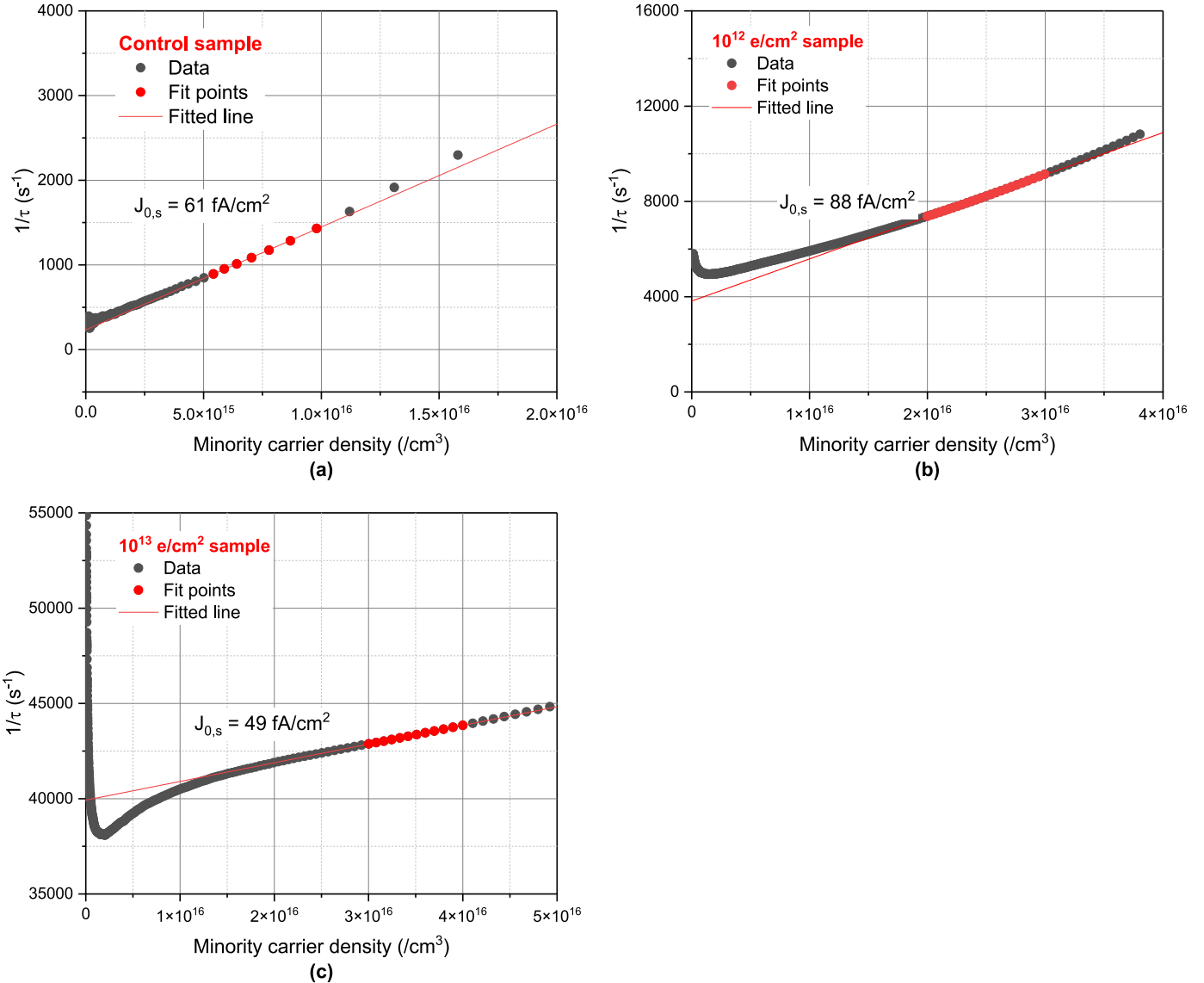


**Fig. 5.** Surface recombination current  $J_0$  fit for (a) control, (b)  $10^{12} \text{ e/cm}^2$  and (c)  $10^{13} \text{ e/cm}^2$  samples.

the lower half of the bandgap, the third candidate of defect energy is located at approximately  $-0.29 \text{ eV}$  with  $k = 3$ . In the deep-level defects region, two possible defect parameters were characterised, with trap energies located at  $-0.29 \text{ eV}$  and  $0.26 \text{ eV}$ , which are found to be similar to the energy range of vacancy-vacancy defect [13,32]. Apart from the defect characterisation with lifetime wafers, the DLTS results of the irradiated PERC solar cell precursor were also investigated in our previous work [33]. Both TIDLS and DLTS indicate that vacancy-related defects are the dominant radiation-induced defects, regardless of cell structure variance and dopant differences.

Overall, the bulk minority carrier lifetime was observed to degrade by approximately one order of magnitude for every one magnitude increase in electron irradiation dose. And this lifetime reduction was likely caused by the vacancy-vacancy defects formed during the electron irradiation process.

### 3.2. Post-irradiation performance of silicon solar cells

The reduction in bulk minority carrier lifetime obviously affects the solar cell performance. Fig. 9 presents the performance of two n-TOPCon silicon solar cells (n-TOPCon-1 and -2) from different manufacturers and one p-PERC silicon solar cell, before and after irradiation by various

fluences of 1 MeV electrons.

As shown in Fig. 9 (a), the post-irradiation efficiency decreases approximately linearly with the logarithmic increase in electron irradiation dose. After exposure to  $10^{12}$ ,  $10^{13}$ , and  $10^{14} \text{ e/cm}^2$  doses of 1 MeV electron flux, the efficiency of n-TOPCon-1 solar cells was reduced from 19.89 % to 18.55 %, 15.30 % and 10.79 %, respectively. The n-TOPCon-2 commercial silicon solar cells, despite having a higher initial efficiency (23.0 %) compared to n-TOPCon-1, degraded to a similar efficiency (10.8 %) after  $10^{14} \text{ e/cm}^2$  electron irradiation. Eventually, the efficiency of n-TOPCon-2 was reduced to 8.7 % after a  $5 \times 10^{14} \text{ e/cm}^2$  irradiation dose. Correspondingly, both the  $J_{\text{SC}}$  and  $V_{\text{OC}}$  of n-TOPCon-2 solar cells degraded with increasing doses of irradiation, retaining  $\sim 24.1 \text{ mA/cm}^2$ , and 543.8 mV after a  $10^{14} \text{ e/cm}^2$  irradiation dose, as shown in Fig. 9(b) and (c). The p-PERC silicon solar cells, in contrast, which exhibited a high initial efficiency of 22.6 %, retained a 16.0 % efficiency after a  $10^{14} \text{ e/cm}^2$  dose. Additionally, its post-irradiation  $J_{\text{SC}}$  and  $V_{\text{OC}}$  were also significantly higher compared to the n-TOPCon cell, which were at  $34.1 \text{ mA/cm}^2$  and 599.8 mV, respectively.

Despite n-TOPCon-1 and n-TOPCon-2 having different initial performances before irradiation, both showed similar post-irradiation efficiencies following a  $10^{14} \text{ e/cm}^2$  1 MeV electron irradiation. In comparison, the p-PERC silicon solar cells demonstrated significantly

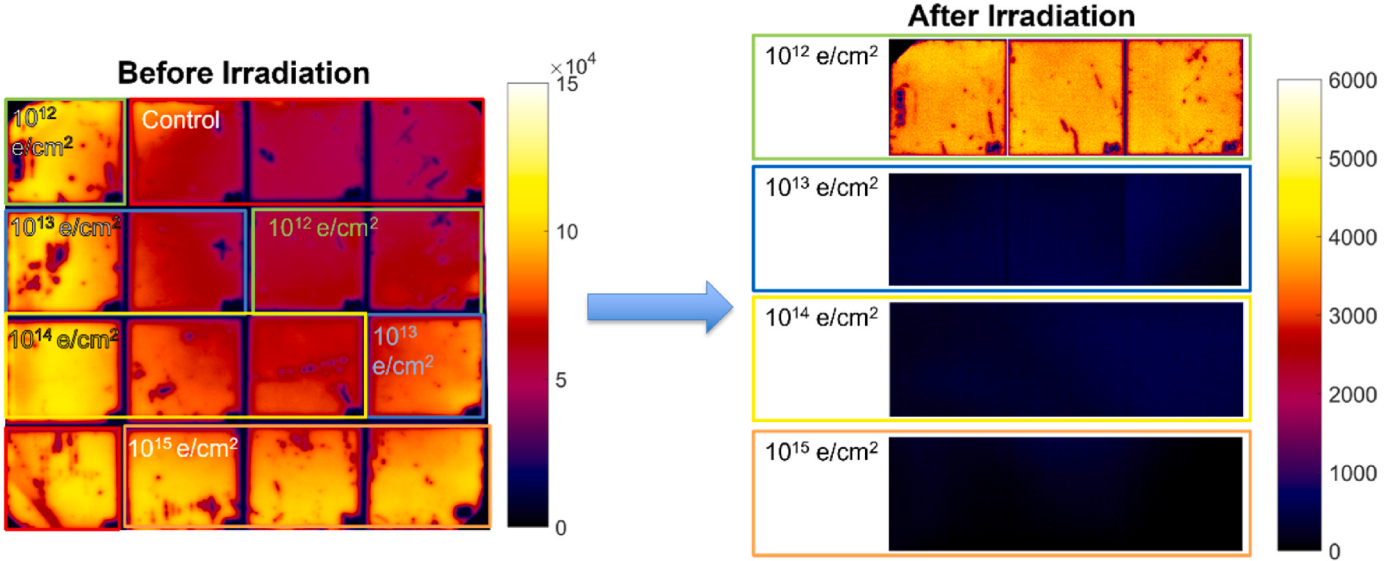


**Fig. 6.** PL images of silicon solar wafer before and after 1 MeV electron irradiation at a total doses of  $10^{12}$   $e/cm^2$ ,  $10^{13}$   $e/cm^2$ ,  $10^{14}$   $e/cm^2$  and  $10^{15}$   $e/cm^2$ , respectively.

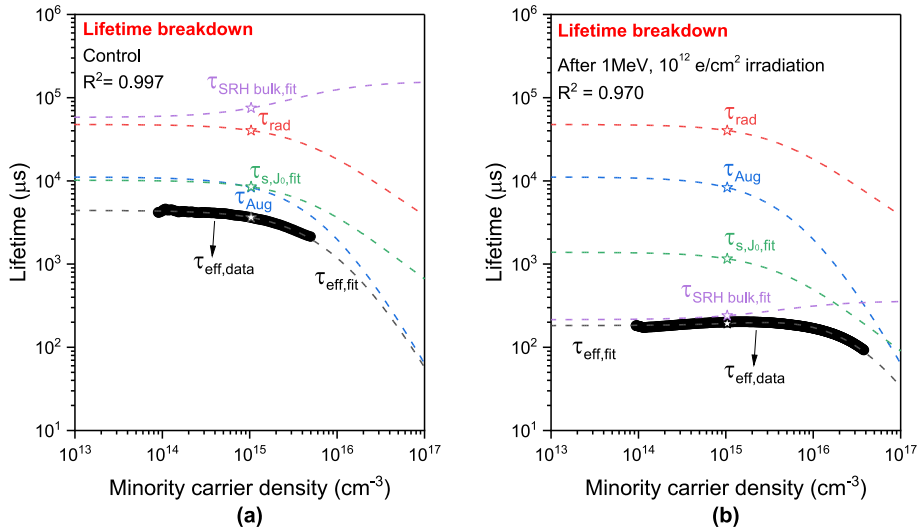


**Fig. 7.** Lifetime curve breakdown for (a) non-irradiated wafer and (b) irradiated wafer after  $10^{12}$   $e/cm^2$  of 1 MeV electron irradiation. The lifetimes at  $\Delta n = 10^{15}$   $cm^{-3}$  are highlighted as hollowed stars.

higher post-irradiation performance after identical irradiation conditions. This enhanced irradiation tolerance can probably be attributed to the greater irradiation tolerance of the p-type substrate compared to n-type [34]. In particular, the use of gallium dopant can lead to an even higher radiation tolerance than a substrate with boron [9] and this was widely used in earlier generations of space silicon solar cell designs [10].

In addition to the post-irradiated cell performance after 1 MeV electron irradiation, the cell performance after 5 MeV electron irradiation is presented in Fig. 10(a). For comparison, this includes commercial n-TOPCon, p-TOPCon, and p-PERC silicon solar cells, along with fitted log-linear trends for efficiency.

As plotted in Fig. 10 (a), the degraded efficiencies were ~12.1 % and 14.4 % for front-illuminated n-TOPCon and p-PERC solar cells, after being exposed to  $2.16 \times 10^{14}$   $e/cm^2$  dose of 5 MeV electrons. Under the same radiation condition, the front-illuminated p-TOPCon solar cells exhibited a more significant reduction in efficiency than the cells with a p-PERC and n-TOPCon structure, which degraded to ~0.4 %. However, when illuminated at the rear, the efficiency of the irradiated p-TOPCon

sample was ~10.08 %. The poor post-radiation performance of the front-illuminated p-TOPCon silicon solar cell was attributed to the rear p-n junction design, which is significantly more sensitive to bulk recombination. This structural influence will be further examined in the subsequent spectral response study.

As the initial performance varies depending on the different silicon solar cells, the corresponding normalised efficiency or remaining factor is presented in Fig. 10 (b) with the fitting curve based on Table 2, allowing us to directly compare the degradation between the fitting curve of 1 MeV results and the 5 MeV electron irradiation. The fitting parameters for the 1 MeV electron irradiation are presented in Table 2 and will be further discussed in next section, where AM0 results are compared to assess cell performance in a real-space environment. For n-TOPCon solar cells, the remaining factor was around ~0.51 after the 5 MeV electron irradiation. Under the same conditions, it was ~0.64, 0.02 and ~0.53 for p-PERC, p-TOPCon (front illumination) and p-TOPCon (rear illumination). Although the p-TOPCon silicon solar cell was not optimised, the rear-illuminated p-TOPCon solar cells still exhibited a

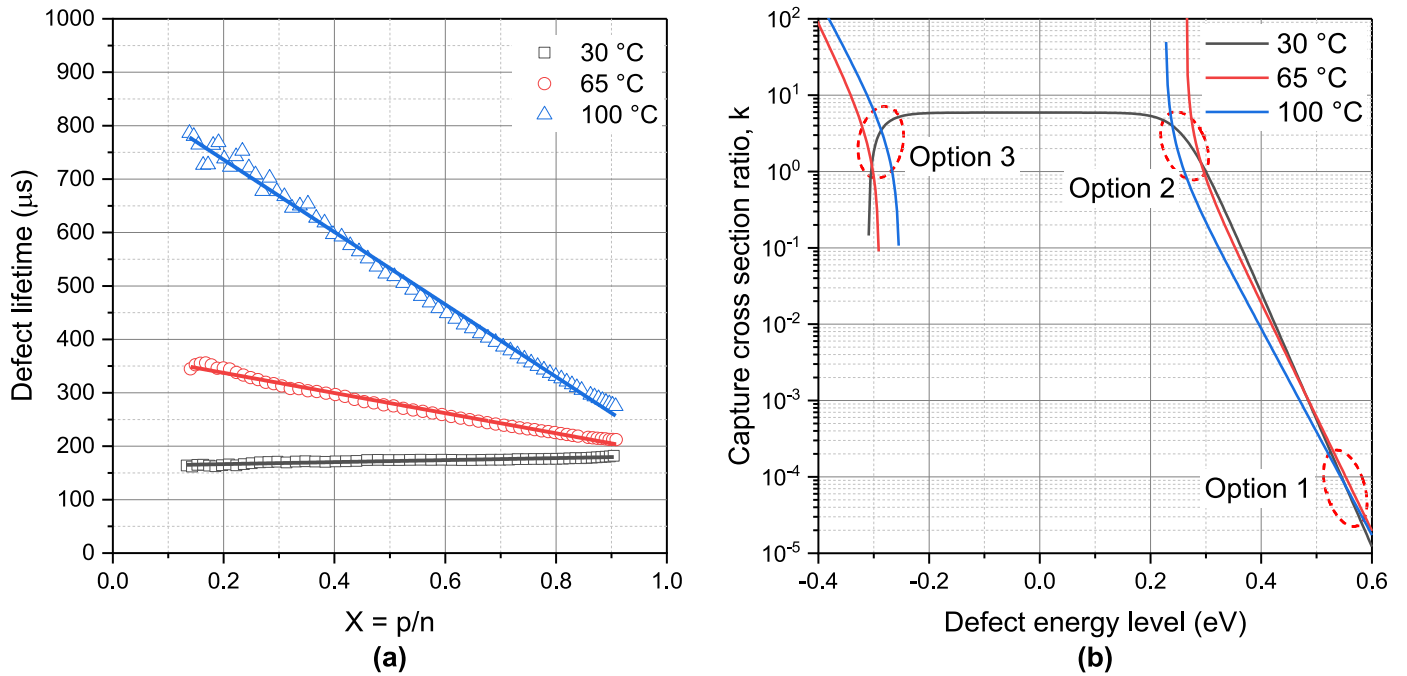


**Fig. 8.** (a) Injection-dependent defect lifetime plotted as a function of  $X = \text{p}/\text{n}$  at 30 °C, 65 °C and 100 °C. (b) capture cross-section ratio as a function of defect energy level (DPSS curve).

**Table 1**

Defect energy level and capture cross-section ratio from DPSS curves generated via TIDLS measurements.

		$E_t - E_i$ (eV)	$k$
Upper half	Option 1	0.55	$7 \times 10^{-5}$
	Option 2	0.26	2.63
Lower half	Option 3	-0.29	3.01

higher remaining factor compared to the n-TOPCon. These results further confirm the superior radiation tolerance of p-type substrates.

Nevertheless, the irradiated p-PERC silicon solar cell (5 MeV and

$2.16 \times 10^{14} \text{ e/cm}^2$ ) achieved a similar post-irradiation performance to cells with  $5 \times 10^{14} \text{ e/cm}^2$  1 MeV irradiation. However, the trend observed in n-TOPCon solar cells was different, where similar post-irradiation performance was obtained after the same doses of 1 MeV and 5 MeV electron irradiation. This may be related to the dopant differences between n-TOPCon and p-PERC silicon solar cells, which lead to a different radiation tolerance responding to the energy of incident electrons.

To further understand the impact of reduced bulk lifetime on silicon solar cells after electron irradiation, Fig. 11 shows EQE curves of the p-PERC, n-TOPCon, and p-TOPCon solar cells measured before and after a dose of  $2.16 \times 10^{14} \text{ e/cm}^2$  5 MeV electrons. The measured data are

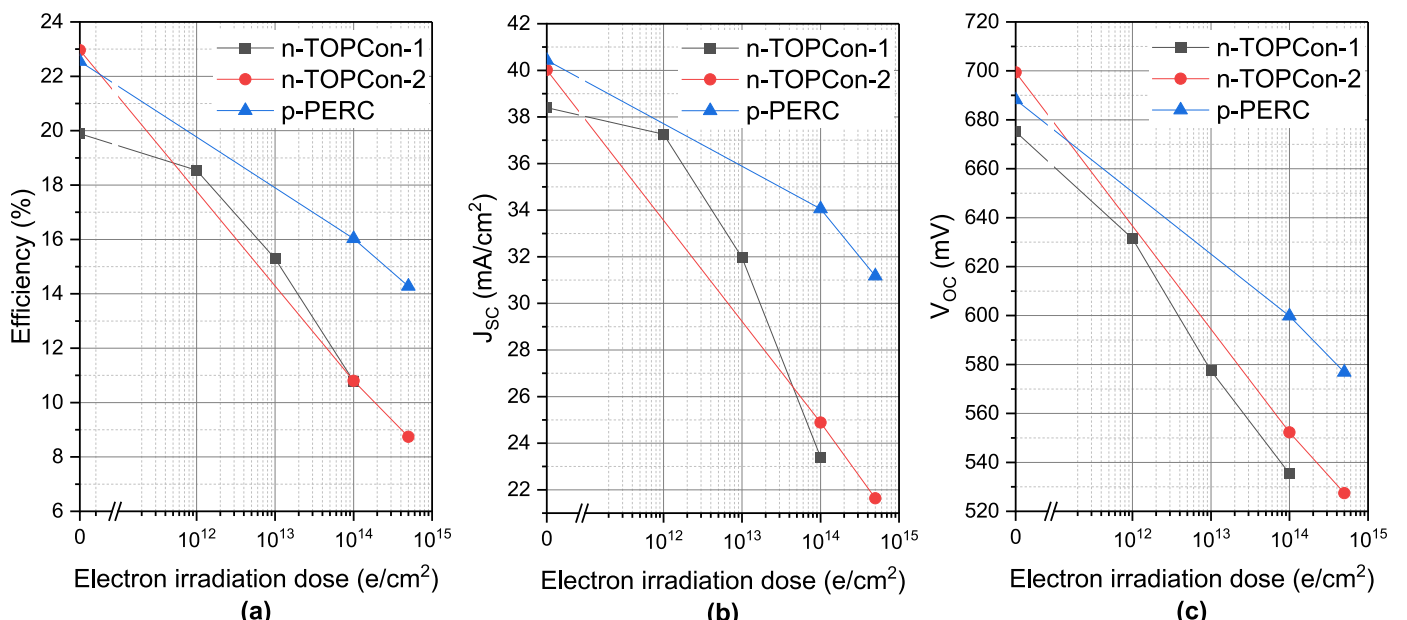


**Fig. 9.** (a) Efficiency, (b)  $J_{\text{SC}}$  and (c)  $V_{\text{OC}}$  as a function of 1 MeV electron dose for n-TOPCon and p-PERC silicon solar cells. The solar cells were measured under the AM1.5g spectrum.

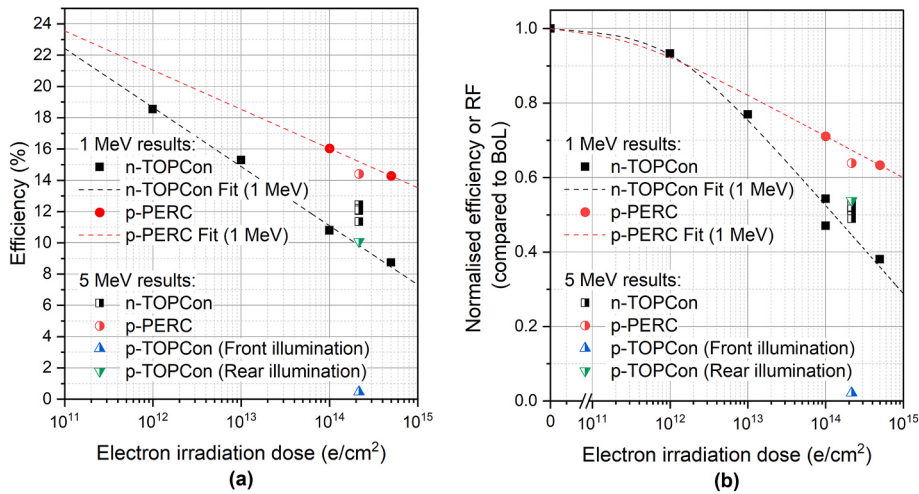


**Fig. 10.** Post-irradiation AM1.5G performance of silicon solar cells after 1 MeV electron and 5 MeV electron irradiation: (a) efficiency and (b) normalised efficiency or RF compared to the BoL performance.

**Table 2**

Fit parameters for the remaining factor of n-TOPCon silicon solar cells and p-PERC silicon solar cells after 1 MeV irradiation.

		Efficiency	V <sub>OC</sub>	J <sub>SC</sub>
n-TOPCon	C	0.238	0.188	0.068
	$\phi_0$	$1.02 \times 10^{12}$	$1.24 \times 10^{12}$	$9.78 \times 10^{10}$
p-PERC	C	0.111	0.104	0.048
	$\phi_0$	$2.54 \times 10^{11}$	$3.11 \times 10^{12}$	$2.03 \times 10^{11}$

presented in hollow circles along with simulated EQE curves in solid lines, generated using a fixed surface recombination parameter ( $J_0 = 50$  fA/cm<sup>2</sup>) for both front and rear skins. The best-fit EQE curves are presented for control (black line) and irradiated (red line) silicon solar cells. Additionally, it is worth noting that the p-n junction of the p-TOPCon silicon solar cell was located on the rear side. Thus, the rear-side illuminated results for p-TOPCon silicon solar cells are also presented for a more representative comparison with the front-illuminated p-PERC and n-TOPCon silicon solar cells.

In Fig. 11(a) and (b) and (d), the trends of EQE degradation were similar among these samples and exhibited a strong wavelength dependence. Following the radiation process, the average EQE values in the wavelength range between 300 nm and 500 nm decreased by only 0.73 %, 2.76 % and 0.31 % for front-illuminated p-PERC, n-TOPCon and rear-illuminated p-TOPCon silicon solar cells, respectively. At longer wavelengths, however, the EQE decreases for higher irradiation doses. In particular, at the wavelength range from 900 nm to 1100 nm, average degradation was observed to be 61.16 % for p-PERC silicon solar cells, 67.52 % reduction for n-TOPCon and 58.60 % for rear-illuminated p-TOPCon.

The Quokka 3 fitted EQE curve fitted with a reduced bulk lifetime shows good agreement with the experimental EQE results of irradiated silicon solar cells. Particularly, the BoL bulk lifetime was found as 510 μs for p-PERC, 600 μs for n-TOPCon and 800 μs for p-TOPCon, respectively. And the as-irradiated bulk lifetime was 0.42–0.43 μs for all our simulations. With decreased bulk electrical lifetime, the notable degradation was observed primarily at wavelengths over 600 nm for the fitted EQE curve. This degradation in long-wavelength EQE is likely attributed to the increased recombination activity during the carrier diffusion. In the front-junction design for p-PERC and n-TOPCon, the long-wavelength photons are typically absorbed and generate excess carriers at a deeper region of the substrate at the opposite side of the p-n junction [35]. These carriers must diffuse across the wafer to the front-side p-n junction for collection, however, the long diffusion path

increases the likelihood of recombination during the transport. As a result, the EQE degradation in irradiated silicon solar cells was more noticeable in the long-wavelength region compared to the short-wavelength spectrum. The fact that the EQE measurements could be reproduced by changing the bulk minority carrier lifetime indicates that a reduction in bulk lifetime is the predominant factor limiting the post-irradiation performance of silicon solar cells. Moreover, it is worth noting that even with similar degraded bulk lifetime, the simulated/experimental EQE of p-PERC and p-TOPCon silicon solar cells remains higher than that of the n-TOPCon silicon solar cell. This could be attributed to the higher effective diffusion length of minority carriers in a p-type substrate, owing to the higher mobility of electrons [36] compared to holes [37].

In contrast, the EQE degradation in front-illuminated p-TOPCon silicon solar cells was observed at short wavelengths. After irradiation, only a small EQE peak of 14.5 % was observed at 1030 nm wavelength, while the overall EQE was reduced by approximately 81 % across the entire wavelength range, as shown in Fig. 11(c). Such a reduction primarily impacts the current generation with short-wavelength light, which is absorbed by the front side of the rear-junction p-TOPCon silicon solar cell. These results suggest that a silicon solar cell with a rear junction design is not the optimal choice for space missions, due to its high sensitivity to the bulk lifetime degradation.

To further investigate the efficiency changes with varying bulk lifetimes, Fig. 12 shows the Quokka 3 simulated efficiency as a function of bulk electrical lifetime for p-PERC, n-TOPCon, and p-TOPCon solar cells. The experimental efficiency results are also plotted as solid dots against the corresponding bulk lifetime values obtained from EQE fitting.

As shown in Fig. 12, the post-irradiation efficiency was estimated to decrease to 13.5 % for p-PERC, 12.5 % for n-TOPCon, 0.8 % for p-TOPCon (front illuminated), and 10.45 % for p-TOPCon (rear illuminated), based on the fitted bulk lifetime at 0.43/0.42 μs from Fig. 11. These simulated efficiency results show a good agreement with the experimental results (solid dots). This consistency suggests that the post-irradiation efficiency is only affected by the decreased bulk minority lifetime caused by radiation damage.

The modelled efficiency of p-PERC, n-TOPCon and p-TOPCon-R gradually increases with a higher bulk lifetime. Eventually, it stabilised at 22.8 %, 23.6 %, and 19.3 % with a bulk lifetime above 10,000 μs, respectively. In contrast, the p-TOPCon with front illumination had a significant bulk lifetime dependence, showing a sharp decline in efficiency when the bulk lifetime degrades below 100 μs. This indicates that the front-illuminated p-TOPCon silicon solar cells appear to be more sensitive to bulk lifetime degradation due to their rear-junction design,

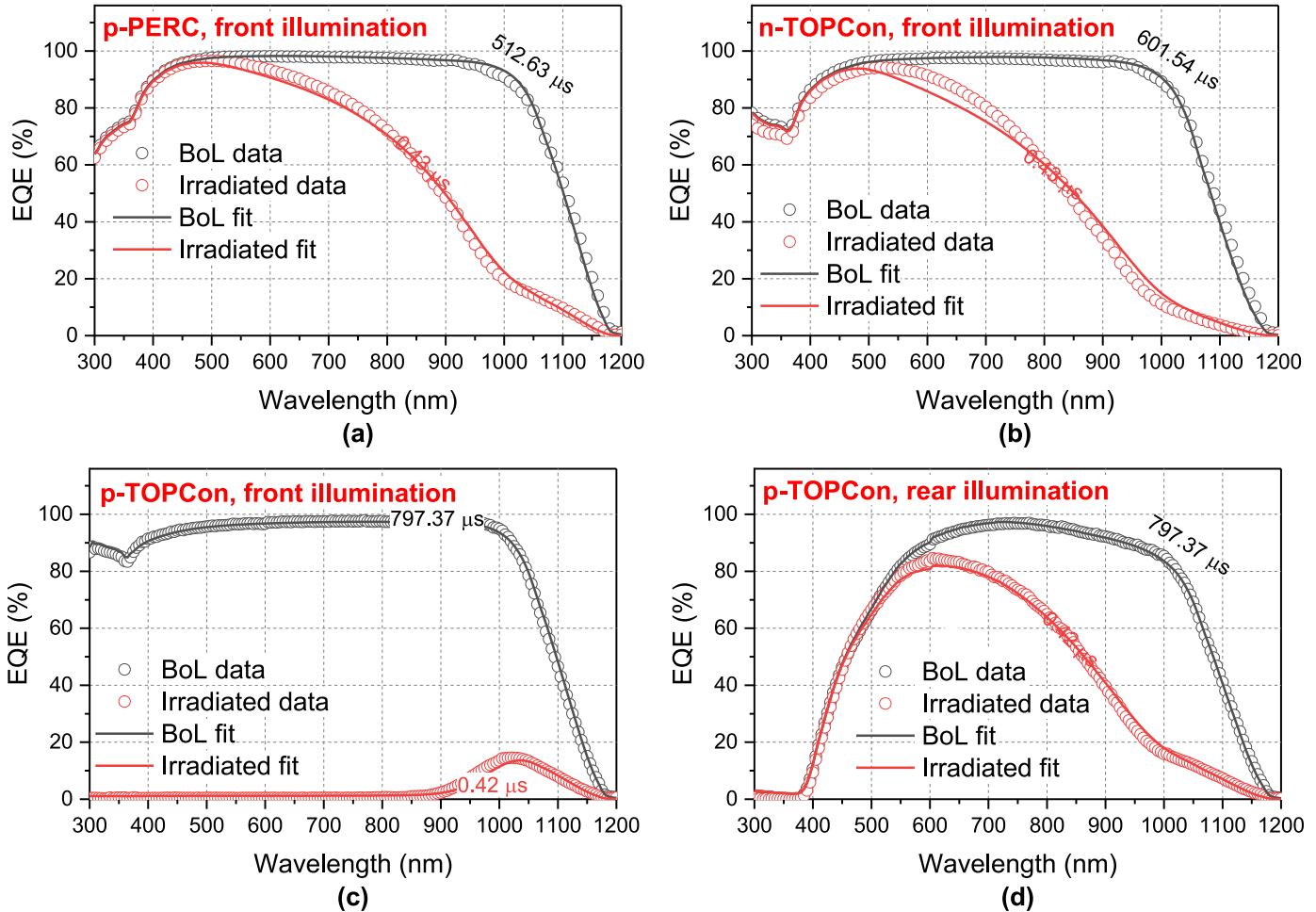


**Fig. 11.** Experimental EQE data and corresponding fitting for non-irradiated and irradiated silicon solar cells ( $2.16 \times 10^{14} \text{ e/cm}^2$  of 5 MeV electrons), (a) p-PERC silicon solar cell with front illumination, (b) n-TOPCon silicon solar cell with front illumination, (c) p-TOPCon silicon solar cell with front illumination, and (d) p-TOPCon silicon solar cell with rear illumination. For clarity, the simulated curves are plotted as solid lines and experimental data are presented as hollow circles. The fitted bulk lifetimes are given as inserts.

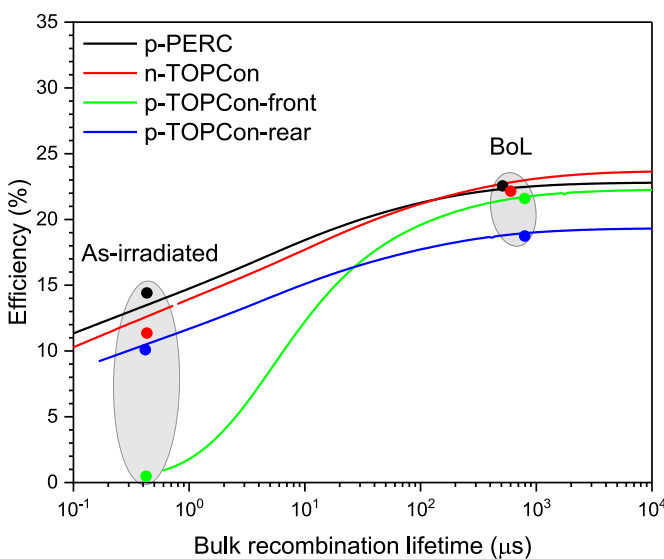


**Fig. 12.** Quokka 3 simulation of cell efficiency as a function of bulk lifetime. The simulated results are plotted as dashed lines, and the experimental results (efficiency) are presented as solid dots.

as mentioned above.

By combining the comprehensive analysis of the lifetime breakdown, EQE, and I-V parameters, it is evident that all these performance losses in irradiated silicon solar cells are consistent with the degradation of bulk minority carrier lifetime. Notably, the p-PERC and p-TOPCon silicon solar cells exhibited a significantly greater irradiation tolerance compared to the n-TOPCon, likely attributed to a higher mobility of minority carriers (electrons) in the p-type substrate than the holes in the n-type substrate. Furthermore, these results suggest that the cell structure with rear-junction design is not suitable for space solar cells, as it is sensitive to the bulk lifetime degradation. It is also worth noting that the remaining factor of all our tested terrestrial silicon solar cells falls below 0.64 following electron irradiation (either 1 MeV &  $5 \times 10^{14} \text{ e/cm}^2$  or 5 MeV &  $2.16 \times 10^{14} \text{ e/cm}^2$ ). This is significantly lower than the RF of  $\sim 0.7$  reported for previous space-specialised silicon solar cells, even after higher irradiation doses (1 MeV &  $10^{15} \text{ e/cm}^2$ ) [11]. Thus, further investigation is required to optimise the current commercial silicon solar cells for space applications.

### 3.3. Operational insights from in-situ satellite solar cell measurements

To give a comparable estimation of irradiation damage during an actual space flight, Fig. 13 shows the performance of the p-PERC solar cells with three different encapsulants during the SSPD-1 space flight [31] with results corrected to standard test conditions (25 °C & 1-sun

illumination). After 310 days in space, the remaining factors of efficiency,  $V_{OC}$  and  $J_{SC}$  for the bare cell were 0.43, 0.63 and 0.80, respectively. For solar cells with a polyimide cover sheet, these values were 0.64, 0.84 and 0.88. In contrast, the similar p-PERC solar cell with a conventional ceria-doped cover glass showed significantly higher irradiation tolerance, with remaining factors of  $\sim 0.98$ , 0.99, and 1 for efficiency,  $V_{OC}$ , and  $J_{SC}$ , respectively, basically showing no significant degradation after 310 days in space. These results highlight that cell encapsulant techniques can provide effective protection for p-PERC silicon solar cells. Particularly, the cover glass may have provided superior protection against protons [38].

Considering the  $J_{SC}$  and efficiency vary significantly due to the illumination incident angle and intensity, the remaining factor of  $V_{OC}$  was used as the most reliable indicator to compare the performance degradation between the simulated and actual space environment, as shown in Fig. 14.

Assuming a constant rate of radiation throughout the space travel, the total irradiation dose scales linearly with the mission length. Thus, these remaining factors can be fitted with Eq. (2.6), and the fitting parameters are presented in Table 3.

As shown in Fig. 14 and Table 3, the fitted curves for the bare silicon solar cells exhibited a faster decline in the remaining factor compared to the silicon solar cells with cover sheets. Based on the fitted results, the bare cell was estimated to decline to the same remaining factor of  $V_{OC}$  as the p-PERC silicon solar cells with  $10^{14}$  e/cm<sup>2</sup> and  $5 \times 10^{14}$  e/cm<sup>2</sup> of 1 MeV electron irradiation after  $\sim 6.4 (\pm 0.7)$  and  $\sim 23.1 (\pm 1.6)$  days of space mission. The required days increased to  $239 (\pm 5)$  and  $894 (\pm 69)$  days for polyimide-capped cells and  $25,500 (\pm 1200)$  and  $93,200 (\pm 4600)$  days for the cells with cover glass. As the encapsulant could partially shield the bare cells from the electron irradiation, the equivalent average dose rate to the bare cell was calculated, as shown in Table 3. Considering an activation energy of  $\sim 1.28$  eV for vacancy-related defects within silicon [39], the potential recovery and annealing behaviour were neglected in the calculation, as the average operational temperature ( $-20^\circ\text{C}$  to  $40^\circ\text{C}$ ) was insufficient to activate such processes.

These results establish a baseline for comparing the SSPD-1 space study and the simulated 1 MeV electron irradiation. It is found that the  $V_{OC}$  degradation caused by a dose of  $5 \times 10^{14}$  e/cm<sup>2</sup> of 1 MeV electron irradiation is equivalent to about 23 days of space irradiation on bare silicon cells. Considering the space silicon solar cells are typically encapsulated for better irradiation tolerance, we believe our simulated irradiation conditions more closely reflect the performance degradation

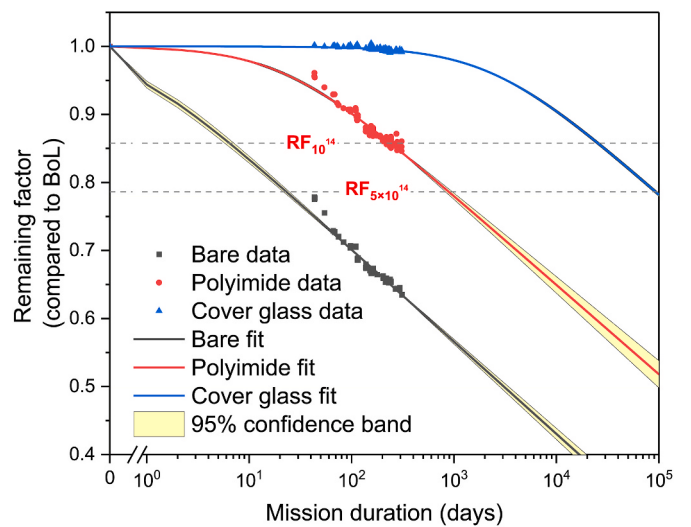


**Fig. 14.**  $V_{OC}$  remaining factor of p-PERC silicon solar cells, along with the fitted curves. The experimental data are presented as solid dots in the graph, and the fitted curves are presented as dashed lines.  $RF_{10}^{14}$  and  $RF_{5 \times 10}^{14}$ : equivalent RF when exposed to  $10^{14}$  and  $5 \times 10^{14}$  e/cm<sup>2</sup> of 1 MeV electron.

**Table 3**

Fitting parameters for  $V_{OC}$  remaining factor of p-PERC silicon solar cells with bare, cover glass and polyimide encapsulation.  $RF_{10}^{14}$  and  $RF_{5 \times 10}^{14}$ : equivalent RF when exposed to  $10^{14}$  and  $5 \times 10^{14}$  e/cm<sup>2</sup> of 1 MeV electron,  $\phi_{ave}$ : equivalent average dose per second to bare cell.

	C	$\phi_0$	Days to $RF_{10}^{14}$	Days to $RF_{5 \times 10}^{14}$	$\phi_{ave}$
Bare	0.136	0.63	$\sim 6.4 \pm 0.7$	$\sim 23.1 \pm 1.6$	$\sim 2.2 \times 10^8$ e/cm <sup>2</sup> /s
Polyimide	0.131	21.48	$\sim 239 \pm 5$	$\sim 894 \pm 69$	$\sim 5.6 \times 10^6$ e/cm <sup>2</sup> /s
Cover glass	0.134	2387.82	$\sim 25,500 \pm$ 1200	$\sim 93,200 \pm$ 4600	$\sim 5.4 \times 10^4$ e/cm <sup>2</sup> /s

expected for a three-to five-year LEO space mission, depending on the encapsulant material and orbit. Furthermore, since the irradiation effect by  $5 \times 10^{14}$  e/cm<sup>2</sup> of 1 MeV electron irradiation is also similar to that by  $2.16 \times 10^{14}$  e/cm<sup>2</sup> of 5 MeV electron irradiation, both irradiation setups

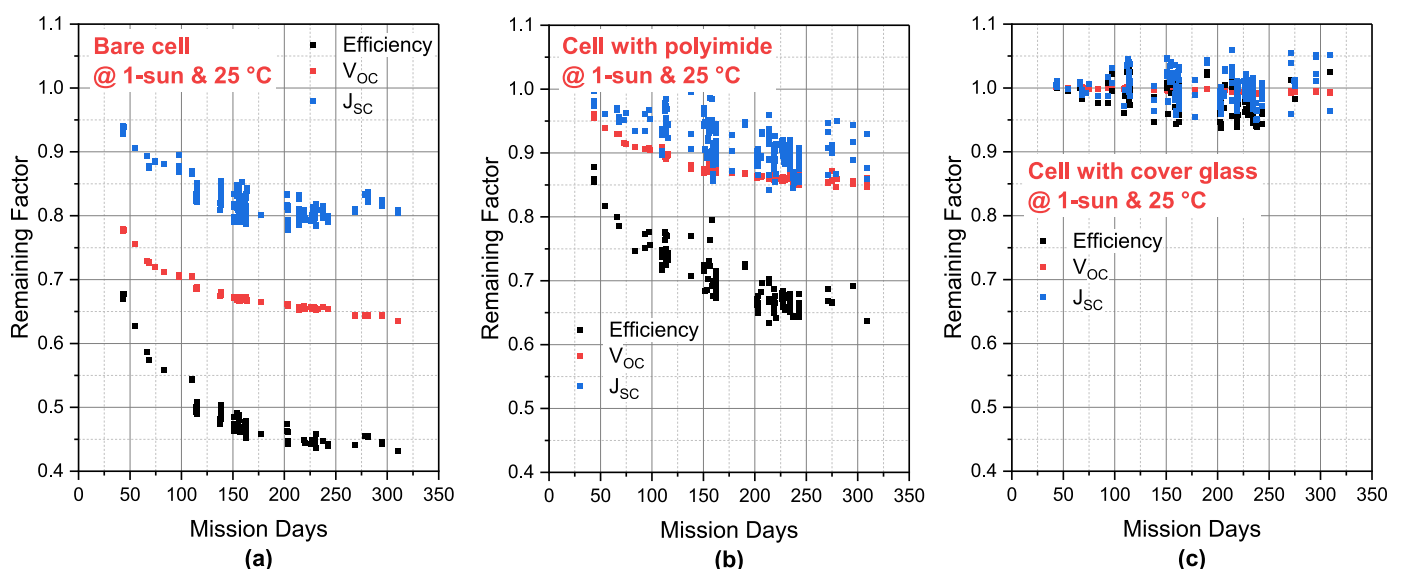


**Fig. 13.** Performance as a function of time for p-PERC silicon solar cell under space environment for (a) bare cell, (b) cell with polyimide and (c) cell with cover glass.

were considered as comparable irradiation conditions.

#### 4. Conclusion

This study investigated the electron irradiation damage on the electrical performance of both silicon lifetime wafers and high-performance p-PERC, n-TOPCon and p-TOPCon commercial silicon solar cells. The PL image results revealed that the electron radiation-induced damage in the silicon solar cell was uniformly distributed across the silicon wafer. After being exposed to 1 MeV electron irradiation at doses ranging from  $10^{12}$  to  $10^{15}$  e/cm<sup>2</sup>, the effective carrier lifetime decreased approximately by an order of magnitude for each order-of-magnitude increase in the dose of 1 MeV electron irradiation, ultimately reaching 0.1 μs for an electron dose of  $10^{15}$  e/cm<sup>2</sup>. Considering the similar  $J_0$  value observed between non-irradiated ( $61\text{ fA}/\text{cm}^2$ ) and irradiated samples ( $88\text{ fA}/\text{cm}^2$ ), and a higher fitted bulk lifetime in the non-irradiated sample (>300 times), the lifetime degradation in bulk was identified as the predominant factor that is affecting the property of the post-irradiation wafer. In addition, recombination active vacancy-vacancy defects were characterised in the lifetime wafer using the TIDLS/DPSS method, leading to a low bulk lifetime in the irradiated samples.

Additionally, significant performance degradation in all types of post-irradiated silicon solar cells was confirmed, due to the degraded electrical performance of the silicon bulk after exposure to both 1 MeV and 5 MeV electron fluxes. The spectra response results further explained how reduced bulk lifetime degradation affects the current generation in irradiated silicon solar cells. Particularly, in a silicon solar cell with standard front-junction design, such as p-PERC and n-TOPCon, the predominant loss of power generation is closely associated with the recombination of photogenerated carriers excited by long-wavelength light. However, in our tested p-TOPCon silicon solar cell, this degradation was particularly pronounced for short-wavelength EQE due to the rear p-n junction design. Thus, a front p-n junction design for silicon space solar cells is more favourable, as it offers a higher overall minority carrier collection, particularly for the carriers generated by short-wavelength photons. However, it should be noted that although the n-TOPCon solar cells had a front junction design and a full rear contact TOPCon structure, their radiation tolerance was still lower than that of the p-PERC and p-TOPCon, which used a gallium-doped substrate known for its higher radiation tolerance. Additionally, the LBSF design in p-PERC silicon solar cell may also increase the possibility of carrier recombination during the extra lateral carrier diffusion.

Finally, by benchmarking the experimental result against the real space mission data from SSPD-1, it was determined that the simulated irradiation condition used in this study ( $5 \times 10^{14}$  e/cm<sup>2</sup> of 1 MeV and  $2.16 \times 10^{14}$  e/cm<sup>2</sup> of 5 MeV) was close to a 3–5 year LEO space mission for an polyimide-encapsulated p-type silicon space solar cell. However, this time estimation varies depending on the specified encapsulation material and orbital setting during travel.

All in all, the bulk carrier lifetime has been confirmed as the predominant factor that limits the performance of irradiated silicon solar cells. And p-PERC, n-TOPCon, and p-TOPCon solar cells demonstrate their advantages and disadvantages for space applications when their bulk lifetime degrades. For these commercial silicon solar cells, further optimisations are required to enhance their post-radiation performance, particularly important for the n-type silicon solar cells, which naturally have weak radiation tolerance.

#### CRediT authorship contribution statement

**Guo Li:** Writing – review & editing, Writing – original draft, Visualization, Validation, Software, Resources, Methodology, Investigation, Formal analysis, Data curation, Conceptualization. **Chukwuka Madumelu:** Writing – review & editing. **Michael Kelzenberg:** Resources. **Peter Toth:** Writing – review & editing. **Gavin Conibeer:** Writing –

review & editing, Supervision, Project administration, Funding acquisition. **Bram Hoex:** Writing – review & editing, Supervision, Project administration, Funding acquisition, Conceptualization.

#### Declaration of competing interest

The authors declare that they have no known competing financial interests or personal relationships that could have appeared to influence the work reported in this paper.

#### Acknowledgements

Guo Li would like to thank the financial support provided by the China Scholarship Council (project ID 202108200014). The authors acknowledge support by the Australian Government through the Australian Research Council's Linkage and Discovery schemes (projects DP220101532, DP170102677, LP210100426 & LP210200883). The authors are grateful to Brendan Wright at UNSW for assisting in the lifetime fitting and to Yan Zhu at UNSW for assisting in the DPSS/TIDLS testing.

#### Data availability

Data will be made available on request.

#### References

- [1] M.A. Green, et al., Solar cell efficiency tables (Version 66), *Prog. Photovoltaics Res. Appl.* 33 (7) (2025) 795–810, <https://doi.org/10.1002/pip.3919>.
- [2] F. Haase, et al., Laser contact openings for local poly-si-metal contacts enabling 26.1%-efficient POLO-IBC solar cells, *Sol. Energy Mater. Sol. Cell.* 186 (2018) 184–193, <https://doi.org/10.1016/j.solmat.2018.06.020>.
- [3] H. Lin, et al., Silicon heterojunction solar cells with up to 26.81% efficiency achieved by electrically optimized nanocrystalline-silicon hole contact layers, *Nat. Energy* 8 (8) (Aug. 2023) 789–799, <https://doi.org/10.1038/s41560-023-01255-2>.
- [4] M. Yamaguchi, K.-H. Lee, K. Araki, N. Kojima, Y. Okuno, M. Imaizumi, Analysis for nonradiative recombination loss and radiation degradation of Si space solar cells, *Prog. Photovoltaics Res. Appl.* 29 (2020), <https://doi.org/10.1002/pip.3346>.
- [5] F. Markus, W. Michael, B. Puzant, 'International technology roadmap for photovoltaic (ITRPV). Machinery and Equipment Manufacturers Association (VDMA), sixteenth ed., 2025 [Online]. Available: <https://itrvp.vdma.org/en/>.
- [6] X. Gao, S. Yang, Z. Feng, Radiation effects of space solar cells, in: X. Wang, Z. M. Wang (Eds.), High-Efficiency Solar Cells: Physics, Materials, and Devices, Springer International Publishing, Cham, 2014, pp. 597–622, [https://doi.org/10.1007/978-3-319-01988-8\\_20](https://doi.org/10.1007/978-3-319-01988-8_20).
- [7] S. Bailey, R. Raffaelle, Space solar cells and arrays, in: *Handbook of Photovoltaic Science and Engineering*, 2003, pp. 413–448, <https://doi.org/10.1002/0470014008.ch10>.
- [8] S.G. Bailey, R. Raffaelle, K. Emery, Space and terrestrial photovoltaics: synergy and diversity, *Prog. Photovoltaics Res. Appl.* 10 (6) (2002) 399–406, <https://doi.org/10.1002/pip.446>.
- [9] A. Khan, et al., Strategies for improving radiation tolerance of Si space solar cells, *Sol. Energy Mater. Sol. Cell.* 75 (1) (2003) 271–276, [https://doi.org/10.1016/S0927-0248\(02\)00169-1](https://doi.org/10.1016/S0927-0248(02)00169-1).
- [10] H. Washio, et al., Development of high efficiency thin silicon space solar cells, in: Conference Record of the Twenty Third IEEE Photovoltaic Specialists Conference - 1993 (Cat. No.93CH3283-9), May 1993, pp. 1347–1351, <https://doi.org/10.1109/PVSC.1993.346922>.
- [11] A. Suzuki, High-efficiency silicon space solar cells, *Sol. Energy Mater. Sol. Cell.* 50 (1) (1998) 289–303, [https://doi.org/10.1016/S0927-0248\(97\)00160-8](https://doi.org/10.1016/S0927-0248(97)00160-8).
- [12] F.-J. Ma, et al., Comparative analysis of radiation-induced effects on the performance of p-type PERC and TOPCon solar cells for space applications, *Sol. Energy Mater. Sol. Cell.* 274 (Aug. 2024) 113002, <https://doi.org/10.1016/j.solmat.2024.113002>.
- [13] M.U. Khan, et al., Degradation and regeneration of radiation-induced defects in silicon: a study of vacancy-hydrogen interactions, *Sol. Energy Mater. Sol. Cell.* 200 (2019), <https://doi.org/10.1016/j.solmat.2019.109990>, 109990–109990.
- [14] A. Fedoseyev, et al., Radiation effects model for ultra-thin silicon solar cells, *J. Phys.: Conf. Ser.* 2675 (1) (Dec. 2023) 012012, <https://doi.org/10.1088/1742-6596/2675/1/012012>.
- [15] 'Solar cell', solestial. <https://solestial.com/product/solar-cell/>. (Accessed 2 November 2025).
- [16] Y. Zhu, Z. Hameiri, Review of injection dependent charge carrier lifetime spectroscopy, *Progress Energy* 3 (1) (2021), <https://doi.org/10.1088/2516-1083/abd488>, 12001–12001.
- [17] A. Cuevas, The effect of emitter recombination on the effective lifetime of silicon wafers, *Sol. Energy Mater. Sol. Cell.* 57 (3) (Mar. 1999) 277–290, [https://doi.org/10.1016/S0927-0248\(98\)00179-2](https://doi.org/10.1016/S0927-0248(98)00179-2).

- [18] J.D. Murphy, K. Bothe, R. Krain, V.V. Voronkov, R.J. Falster, Parameterisation of injection-dependent lifetime measurements in semiconductors in terms of Shockley-Read-Hall statistics: an application to oxide precipitates in silicon, *J. Appl. Phys.* 111 (11) (Jun. 2012) 113709, <https://doi.org/10.1063/1.4725475>.
- [19] A. Richter, S.W. Glunz, F. Werner, J. Schmidt, A. Cuevas, Improved quantitative description of Auger recombination in crystalline silicon, *Phys. Rev. B* 86 (16) (2012), <https://doi.org/10.1103/PhysRevB.86.165202>, 165202–165202.
- [20] P.P. Altermatt, F. Geelhaar, T. Trupke, X. Dai, A. Neisser, E. Daub, Injection dependence of spontaneous radiative recombination in c-Si: experiment, theoretical analysis, and simulation, in: NUSOD '05. Proceedings of the 5th International Conference on Numerical Simulation of Optoelectronic Devices, 2005, pp. 47–48, <https://doi.org/10.1109/NUSOD.2005.1518128>. Sep. 2005.
- [21] G.P. Summers, E.A. Burke, P. Shapiro, S.R. Messenger, R.J. Walters, Damage correlations in semiconductors exposed to gamma, electron and proton radiations, *IEEE Trans. Nucl. Sci.* 40 (6) (Dec. 1993) 1372–1379, <https://doi.org/10.1109/23.273529>.
- [22] Screened relativistic (SR) treatment for displacement damage NIEL doses (TNID) and nuclear stopping powers in materials; sr-framework for electronic stopping powers and restricted energy-losses, ionizing doses (TID); residual particle energy traversing shielding materials; single event effects (SEE) and Weibull functional form. <https://www.sr-niel.org/>. (Accessed 26 July 2025).
- [23] C. Leroy, P.G. Rancoita, *Principles of Radiation Interaction in Matter and Detection*, World Scientific, 2004.
- [24] S.R. Messenger, G.P. Summers, E.A. Burke, R.J. Walters, M.A. Xapsos, Modeling solar cell degradation in space: a comparison of the NRL displacement damage dose and the JPL equivalent fluence approaches, *Prog. Photovoltaics Res. Appl.* 9 (2) (2001) 103–121, <https://doi.org/10.1002/pip.357>.
- [25] H.Y. Tada, J.R. Carter, B.E. Anspaugh, R.G. Downing, *Solar Cell Radiation Handbook*, NASA-CR-169662, Nov. 1982 [Online]. Available: <https://ntrs.nasa.gov/citations/19830006416>. (Accessed 27 July 2025).
- [26] A. Fell, A free and fast three-dimensional/two-dimensional solar cell simulator featuring conductive boundary and quasi-neutrality approximations, *IEEE Trans. Electron. Dev.* 60 (2) (Feb. 2013) 733–738, <https://doi.org/10.1109/TED.2012.2231415>.
- [27] A. Fell, J. Schön, M.C. Schubert, S.W. Glunz, The concept of skins for silicon solar cell modeling, *Sol. Energy Mater. Sol. Cell.* 173 (2017) 128–133, <https://doi.org/10.1016/j.solmat.2017.05.012>.
- [28] A. Fell, P.P. Altermatt, A detailed full-cell model of a 2018 commercial PERC solar cell in Quokka3, *IEEE J. Photovoltaics* 8 (6) (2018) 1443–1448, <https://doi.org/10.1109/JPHOTOV.2018.2863548>.
- [29] A. Fell, et al., Modeling parasitic absorption in silicon solar cells with a near-surface absorption parameter, *Sol. Energy Mater. Sol. Cell.* 236 (Mar. 2022) 111534, <https://doi.org/10.1016/j.solmat.2021.111534>.
- [30] Home | Quokka3. <https://www.quokka3.com/>. (Accessed 22 May 2025).
- [31] A. Fikes, et al., The caltech space solar power demonstration one mission, in: 2022 IEEE International Conference on Wireless for Space and Extreme Environments (WiSEE), Oct. 2022, pp. 18–22, <https://doi.org/10.1109/WiSEE49342.2022.9926883>.
- [32] A. Khan, M. Yamaguchi, S.J. Taylor, T. Hisamatsu, S. Matsuda, Effects of Annealing on Type Converted Si and Space Solar Cells Irradiated with Heavy Fluence 1 MeV Electrons, *Jpn. J. Appl. Phys.* 38 (5R) (1999), <https://doi.org/10.1143/jjap.38.2679>, 2679–2679.
- [33] G. Li, et al., Rapid healing: how hydrogenation supercharges recovery of electron-irradiation defects in Ga-doped PERC solar cells, *Sol. Energy Mater. Sol. Cell.* 290 (Sep. 2025) 113729, <https://doi.org/10.1016/j.solmat.2025.113729>.
- [34] A. ur Rehman, S.H. Lee, S.H. Lee, Silicon space solar cells: progression and radiation-resistance analysis, *J. Kor. Phys. Soc.* 68 (4) (2016) 593–598, <https://doi.org/10.3938/jkps.68.593>.
- [35] M.A. Green, *Silicon Solar Cells: Advanced Principles & Practice*, Centre for Photovoltaic Devices and Systems, 1995.
- [36] A.B. Sproul, M.A. Green, Intrinsic carrier concentration and minority-carrier mobility of silicon from 77 to 300 K, *J. Appl. Phys.* 73 (3) (Feb. 1993) 1214–1225, <https://doi.org/10.1063/1.353288>.
- [37] S.E. Swirhun, J.A. del Alamo, R.M. Swanson, Measurement of hole mobility in heavily doped n-type silicon, *IEEE Electron Device Lett.* 7 (3) (Mar. 1986) 168–171, <https://doi.org/10.1109/EDL.1986.26333>.
- [38] P. Kwak, N. Kim, J. Kim, D. Kim, K. Song, J. Lee, Flexible space solar cell array with radiation shield fabricated by guided-printing of cover glasses, *Sol. Energy Mater. Sol. Cell.* 169 (Sep. 2017) 210–214, <https://doi.org/10.1016/j.solmat.2017.05.019>.
- [39] M. Mikelsen, E.V. Monakhov, G. Alfieri, B.S. Avset, B.G. Svensson, Kinetics of divacancy annealing and divacancy-oxygen formation in oxygen-enriched high-purity silicon, *Phys. Rev. B* 72 (19) (Nov. 2005) 195207, <https://doi.org/10.1103/PhysRevB.72.195207>.